Faraday Discussions

Cite this: *Faraday Discuss.*, 2017, **197**, 421

PAPER

Time- and space-resolved study of the methanol to hydrocarbons (MTH) reaction – influence of zeolite topology on axial deactivation patterns†

Daniel Rojo-Gama,[ab] Samaneh Etemadi,[a] Eliot Kirby,[a] Karl Petter Lillerud,[a] Pablo Beato,*[b] Stian Svelle[a] and Unni Olsbye*[a]

Received 8th September 2016, Accepted 10th October 2016
DOI: 10.1039/c6fd00187d

Zeolites representing seven different topologies were subjected to life-time assessment studies as methanol to hydrocarbons (MTH) catalysts at 400 °C, P(MeOH) = 13 kPa and P(tot) = 100 kPa. The following topologies were studied: ZSM-22 (TON), ZSM-23 (MTT), IM-5 (IMF), ITQ-13 (ITH), ZSM-5 (MFI), mordenite (MOR) and beta (BEA). Two experimental approaches were used. In the first approach, each catalyst was tested at three different contact times, all giving 100% initial conversion. The life-time before conversion decreased to 50% at each contact time was measured and used to calculate critical contact times (*i.e.* the contact time needed to launch the autocatalytic MTH reaction) and deactivation rates. It was found that the critical contact time is strongly correlated with pore size: the smaller the pore size, the longer the critical contact time. The second experimental approach consisted of testing the catalysts in a double tube reactor with 100% initial conversion, and quenching the reaction after 4 consecutive times on stream, representing full, partial, and zero conversion. After quenching, the catalyst bed was divided into four segments, which were individually characterised for coke content (temperature-programmed oxidation) and specific surface area (N_2 adsorption). The axial deactivation pattern was found to depend on pore size. With increasing pore size, the main source of coke formation changed from methanol conversion (1D 10-ring structures), to partly methanol, partly product conversion (3D 10-ring structures) and finally mainly product conversion (3D 12-ring structure). As a result, the methanol conversion capacity changed little with contact time for ZSM-5, while it increased with increasing contact time for the catalysts with smaller pore sizes, and decreased with increasing contact time for pore sizes larger than ZSM-5.

[a]*Center for Materials Science and Nanotechnology (SMN), Department of Chemistry, University of Oslo, P.O. Box 1033, Blindern, N-0315 Oslo, Norway. E-mail: unni.olsbye@kjemi.uio.no*

[b]*Haldor Topsøe A/S, Haldor Topsøes Allé 1, 2800 Kgs. Lyngby, Denmark. E-mail: pabb@topsoe.dk*

† Electronic supplementary information (ESI) available. See DOI: 10.1039/c6fd00187d

1. Introduction

The conversion of methanol to hydrocarbons (MTH) provides an efficient route for the production of valuable chemicals and liquid fuels from low cost carbon feedstocks such as natural gas, coal or biomass.[1,2] The MTH reaction is catalyzed by zeolites, crystalline aluminosilicates possessing strong Brønsted acidity dispersed within a microporous network, leading to shape selective catalysis.[3] The hydrocarbons formed in the MTH reaction consist of a mixture of mainly light olefins and aromatic species, and some paraffins[4] resulting from an autocatalytic complex reaction network.[2] The autocatalytic nature of the MTH reaction involves the methylation and subsequent cracking/dealkylation of adsorbed alkenes and arenes as the main reaction steps.[5,6]

In addition to the targeted products, the accumulation of coke residues in the micropores and on the outer surface of the zeolite triggers a decrease in the catalyst activity with time on stream.[7–9] The catalytic performance with respect to product selectivity and deactivation depends on the zeolite topology and operating conditions of the MTH reaction.[2,7,10] Deactivation as a result of coke deposition is reversible, and coke residues can be removed by oxidative regeneration at 300–600 °C leading to a recovery of the catalytic activity.

Great effort has been made in recent years to gain knowledge about deactivation phenomena in the MTH reaction.[7,9,11–18] Most studies have been carried out *ex situ*, analyzing the post-mortem coke content and accompanying loss of accessible surface area in the entire catalyst bed. However, when an autocatalytic reaction like MTH is carried out in a fixed bed plug flow reactor, an axial deactivation gradient is expected. Under conditions where full initial conversion is achieved, the catalyst bed can be divided into three sequential reaction zones. The feed inlet segment is defined as the initiation zone. In this first zone, partial conversion of methanol to dimethyl ether (DME), as well as a slow formation and accumulation of autocatalytic species (alkenes and arenes) take place. When sufficient autocatalytic species have been produced, the autocatalytic reaction dominates product formation, and this next zone is called the autocatalytic zone. Finally, in the product zone, located towards the bed outlet, oxygenates are fully consumed and only hydrocarbon interconversion reactions take place.[7,19]

A few studies have taken into account the axial mode of zeolite deactivation when the MTH reaction is carried out in a fixed bed plug flow reactor. Haw and Marcus proposed a "burning cigar model" to describe the deactivation and inhomogeneous aging of SAPO-34, in which a layer of active catalyst moves along the bed with increasing time on stream, leaving the deactivated catalyst in its wake.[20] This model was later confirmed by Wragg *et al.*, who used operando time- and space-resolved X-ray diffraction to monitor the deactivation of SAPO-34 as an MTH catalyst. Moreover, Wragg *et al.* allocated the initial increase in methanol conversion with time on stream over this particular catalyst to the slow accumulation of autocatalytic species in the initiation zone, which gradually transformed it into an autocatalytic zone.[21] In another contribution, Schulz studied the MTH reaction over ZSM-5 at 475 °C, also in a plug flow reactor, and visually observed that the spent catalyst was inhomogeneously deactivated.[9] The top part, which was heavily deactivated due to coke located on the outer surface of the catalyst particles, was followed by a grey reaction zone, whereas a less deactivated

zone with a light blue color was observed towards the end of the bed. This color was allocated to "coke seeds", formed by secondary reactions of the MTH products.

Recently, Bleken *et al.*[14] investigated the deactivation of a microporous ZSM-5 catalyst as well as its desilicated analogue by dividing the partially deactivated catalyst bed into different segments that were subsequently characterized. They observed that desilication treatment not only improved the catalyst lifetime, but also altered the axial deactivation pattern. For the microporous parent sample, the layers located near the entrance of the catalyst bed were most severely deactivated. However, in the desilicated, meso-/micro-porous sample, the axial deactivation pattern was more homogenous and the layers at the bottom of the bed were slightly more deactivated than the preceding layers. Notably, this observation demonstrated that the axial deactivation pattern observed in previous contributions is not globally applicable to all MTH catalysts. This observation served as an inspiration for the current study.

A similar approach to the one used by Bleken *et al.* was presented by Luo *et al.*[22] who investigated the spatial and temporal evolution of confined species in SAPO-34. The authors concluded that methanol and olefins led to the formation of intermediate species, which were subsequently transformed into coke.

Very recently, another approach was applied by Müller *et al.*[13] who compared the deactivation rate of a ZSM-5 catalyst in two different reactors; a plug-flow reactor (PFR) and a continuously stirred tank reactor (CSTR). Notably, the catalyst deactivated substantially faster in the PFR, leading the authors to suggest that coke formation from methanol alone is a major source of catalyst deactivation. In an earlier contribution from the same group (the Lercher group), Sun *et al.* observed a dramatic increase in catalyst conversion capacity when butanol was co-fed with methanol over ZSM-5.[23] Together, these observations led Lercher *et al.* to revisit and support an early proposal by Hutchings *et al.*,[24] *i.e.* that coke formation in the MTH reaction is preceded by hydrogen transfer between two methanol molecules, leading to the formation of formaldehyde and methane (reaction (1)). Formaldehyde is subsequently converted to coke species. Furthermore, Lercher *et al.* suggested that Rx. (1) is inhibited by the presence of hydrocarbons.

$$2CH_3OH \rightarrow CH_4 + CH_2O \quad (1)$$

Other possible coke forming mechanisms which are supported by experimental results in the literature are reactions between methanol and hydrocarbon pool species, such as polymethyl benzene, leading *e.g.* to the hepta-methyl benzenium cation which can subsequently rearrange into a naphtalene precursor (reaction (2))[25,26]

$$C_6(CH_3)_6 + CH_3OH + H^+ \rightarrow C_6(CH_3)_7{}^+ + H_2O \rightarrow \rightarrow C_{10}H_5(CH_3)_3 + 6\text{"H"} + H_2O + H^+ \quad (2)$$

as well as reactions between hydrocarbon pool species leading again to the formation of polycyclic coke precursors, as exemplified by reaction (3)[20,27]

$$C_6H_6 + 2C_3H_6 \rightarrow\rightarrow C_{10}H_6(CH_3)_2 + 6\text{"H"} \quad (3)$$

All three classes of reactions are expected to contribute to coke formation in the MTH reaction. However, it is of interest to study to which extent the relative importance of these three reaction classes depends on catalyst topology.

Among the mathematical models put forward to simulate MTH catalyst deactivation, the models of Janssens[11] and Janssens *et al.*[12] are of particular relevance for this study. Both models consider deactivation simply as a loss of effective contact time with time on stream. The Janssens model[11] was initially developed for the commercially used ZSM-5 catalyst, and the approach resulted from the observation that the variation in product yield over ZSM-5, in particular an increase in ethene and propene yield before methanol breakthrough, was similar to the evolution of the products at an increasing space velocity.[28] A preassumption of this model is that deactivation is non-selective, *i.e.* the individual product yields obtained at a given conversion level are the same in a fresh catalyst as in a partially deactivated catalyst. This preassumption has been validated for ZSM-5,[29] ZSM-22, ZSM-23, EU-1[30] and SAPO-5[31] catalysts. A further assumption of Janssens' model is that the deactivation rate is first order in methanol and proportional to methanol conversion. These assumptions mean that coke formation from products alone is negligible (an assumption which was supported by the experimental evidence on ZSM-5 (*vide supra*)) and furthermore, that the selectivity for coke formation is constant from zero to full methanol conversion. Janssens' model was successfully applied to correlate the deactivation of a large set of ZSM-5 catalysts to their initial activity and deactivation rate.[32] However, a limitation of Janssens' first model is that it does not take into account the autocatalytic nature of the MTH reaction and hence, the more complex correlation between applied contact time and methanol conversion capacity for catalysts with a non-negligible initiation zone. This limitation was addressed by the autocatalytic deactivation model which was subsequently developed by Janssens *et al.*[12] based on the observation that the conversion capacity of ZSM-22 as an MTH catalyst increases linearly with an increase in the applied contact time, τ_0, *i.e.* with the ratio between the catalyst weight and total gas flow (W/F).

In the autocatalytic deactivation model, the rate of methanol conversion is expressed as:

$$\mathrm{d}M/\mathrm{d}\tau = -k_1 M - k_2 MP \tag{4}$$

where: M is methanol concentration and P is product concentration. Such a simplified expression is warranted by the stable steady-state product distribution reported for many MTH catalysts in the 0–80% conversion range.[33] Mathematical manipulation led to the following simplified correlation between the catalyst lifetime, $t_{1/2}$, and the deactivation coefficient (a), leading to a decrease in the conversion from 100% to 50%:

$$t_{1/2} = (\tau_0 - \tau_{\mathrm{crit}})/a \tag{5}$$

where: τ_0 is the applied contact time (W/F) and τ_{crit} is the critical contact time, *i.e.* the contact time needed to build up sufficient autocatalytic pool species to launch the autocatalytic reaction. Excellent correlation between eqn (5) and the catalyst conversion capacity was found for a ZSM-22 catalyst.[12]

The aim of this work was to elucidate the influence of zeolite topology on the axial mode of deactivation during the MTH reaction. The topologies studied comprise 1D 10-ring structures (ZSM-22, ZSM-23), 3D 10-ring structures (ZSM-5, IM-5, ITQ-13), a 1D 12-ring zeolite (mordenite) and a 3D 12-ring structure (beta). Two approaches were used: first, the methanol conversion capacity of each topology was studied at different contact times. The autocatalytic deactivation model (*vide supra*) was applied to all materials, in order to elucidate critical contact times and deactivation rates. Furthermore, a selection of the materials was subjected to life-time performance studies in a double tube reactor, where segments of the catalyst bed could be characterized separately after selected times on stream. The study revealed that the influence of hydrocarbon products as coke precursors increases with increasing pore size. As such, the catalyst conversion capacity increases with increasing contact time for smaller-pore 10-ring zeolites such as H-ZSM-22 and H-ZSM-23, in which coke is mainly formed from methanol, whereas it decreases with increasing contact time for larger 12-ring pore zeolites, such as beta zeolite. The study further suggested a correlation between pore size and critical contact time.

2. Experimental

2.1 Catalysts

Eight zeolite samples were tested in the first part of the study, where catalyst deactivation was studied as a function of applied contact time, according to the autocatalytic deactivation model. Most samples were obtained from commercial producers; ZSM-22 (Zeolyst), ZSM-23 (Zeolyst), mordenite-14386 (Ventron), ZSM-5 (Pentasil and MFI-27; both from Süd-Chemie) and beta (VALFOR CP806; Zeolyst); while IM-5 and ITQ-13 were synthesized under hydrothermal conditions as reported elsewhere.[34,35]

For the spatio-temporal investigation, the following seven zeolite samples were used: ZSM-5 (MFI-27; Süd-Chemie), beta (VALFOR CP-806, CP-7119 and CP-814E; all from Zeolyst) and mordenite (CBV-21A, Zeolyst) were obtained from commercial producers, while ZSM-22 and ZSM-23 were synthesized in-house following a previously reported experimental procedure.[36,37]

All materials were ion-exchanged with a 1 M NH_4NO_3 solution 3 × 2 h in a 75 °C water bath, followed by calcination in static air at 550 °C for 5 hours to obtain the protonated form.

2.2 Catalyst characterization

The crystallinity and purity of the fresh materials were determined using powder X-ray diffraction, collected on a Siemens Bruker D5000 using Bragg-Brentano geometry and $CuK_{\alpha 1}$ radiation (λ = 1.5406 Å). The experimental results were analyzed by full-profile Le Bail refinement.

The elemental composition of the zeolites was obtained using X-ray micro-analysis (SEM/EDX).

N_2 adsorption isotherms were measured at −196 °C, using a Belsorp-mini II instrument. Prior to each measurement, fresh samples were outgassed under vacuum for 1 h at 80 °C and for 4 h at 300 °C. Spent catalysts were outgassed for 4 hours, 1 h at 80 °C and 3 h at 180 °C. Specific surface area was calculated using the BET equation[38] in the range of validity for microporous materials.[39]

FT-IR measurements were performed on fresh catalysts on a Bruker Vertex 80 with an MCT detector operating in transmission mode. Before the measurement, samples were pressed into a self-supporting wafer and were pre-treated under vacuum at 150 °C for 1 h, at 300 °C for 1 h and at 450 °C for 1 h. For CO adsorption, samples were cooled to −196 °C. After complete adsorption of CO, spectra were recorded during CO desorption.

The total amount of coke in the deactivated catalysts was obtained using TGA on a Rheometric Scientific STA 1500 instrument. Approximately 15 mg of sample was heated to 800 °C using a heating rate of 5 °C min^{-1} in 25 mL min^{-1} of synthetic air. Then, the final hold time at this temperature was 40 minutes. The coke content was normalized to the amount of zeolite used in each experiment.

The coke species retained in the catalyst after methanol conversion were analyzed by the dissolution–extraction technique.[40] Approximately 15 mg of the deactivated catalyst was dissolved in 1 mL of 15% HF for 60 minutes, inside a small capped Teflon vial. Subsequently, the soluble fraction of the coke was extracted with 1 mL of CH_2Cl_2 and analyzed with an Agilent 6890N/5793 MSD GC-MS equipped with an HP-5MS column (60 m, 0.25 mm i.d., stationary phase thickness 0.25 μm). *ortho*-Chloro-toluene was used as the internal standard to normalize all chromatograms. The NIST98 database was used for the identification of species.

2.3 Catalytic tests

Two reactor setups were used for the catalytic tests. To investigate the influence of contact time on catalyst deactivation, a U-shaped fixed-bed quartz reactor (8 mm i.d.) and 50 mg of catalyst (250–420 μm) was used.

For the spatio-temporal study, a double-tube straight quartz reactor (9 mm i.d. and 11 mm o.d.) was chosen. 200 mg of catalyst (250–420 μm) was poured in the internal reactor using quartz wool as a support for the catalyst bed. After thermal quenching at increasing times on stream, the catalyst bed was subsequently divided into 4 layers, being numbered consecutively from the entrance to the outlet of the catalyst bed.

Regardless of the reactor setup, catalytic experiments were carried out at ambient pressure and 400 °C. Prior to the catalytic tests, the reactor was heated to 550 °C under He flow. At this temperature, catalysts were calcined for 1 h in a flow of pure O_2. Then, the temperature was lowered to 400 °C, the actual reaction temperature, using He. MeOH (BDH Laboratory, purity > 99.8%) was fed to the reactor by flowing a stream of He through a methanol evaporator kept at 293 °C ($P_{MeOH} = 13$ kPa). The contact times (τ = catalyst mass/total gas flow [g h mol^{-1}]) were modified by adjusting the flow of He accordingly, keeping the amount of catalyst constant in each test. The reaction effluent was analyzed online using an Agilent 6890 gas chromatograph equipped with a flame ionization detector and an Agilent J&W capillary column (length 60 m, 0.530 mm i.d., stationary phase thickness of 20 μm). Conversion, selectivity and product yield were calculated on C_1 basis as described in literature.[41]

3. Results

All catalytic tests reported in this study were performed at contact times leading to 100% initial conversion. Representative conversion *versus* time on stream plots

for the zeolite topologies which were subjected to spatio-temporal studies are shown in Fig. 1. It should be noted that the applied contact time, τ_0, required to obtain full initial conversion is different for each catalyst, and that the data in Fig. 1 were therefore obtained at different applied contact times (*vide infra*).

Fig. 2 shows the change of methanol conversion capacity (in g MeOH per g catalyst) for each of the materials tested at different applied contact times. The data in Fig. 2 were obtained by integrating the area under the conversion *versus* time on stream curves until complete deactivation. The catalyst lifetime to 50% MeOH conversion, $t_{1/2}$, is plotted *versus* the applied contact time, τ_0, for each catalyst in Fig. 3. As a general comment, the results in Fig. 3 show that $t_{1/2}$ depends linearly on the applied contact time for all zeolites, as predicted by the autocatalytic deactivation model.[12] Using this model, the deactivation constant (a) and the critical contact time (τ_{crit}) were derived from the data in Fig. 3, using eqn (5). The slope of the $t_{1/2}$ *versus* τ_0 line equals $1/(a)$ and the critical contact time is obtained by extrapolating the line to $t_{1/2} = 0$. Results of a and τ_{crit} are presented in Table 1.

In the following sections, data obtained for each zeolite topology will be presented separately, followed by an overall discussion of the results, finally leading to the conclusion of the study. Characterization data for the zeolite samples tested in this study can be found in Table 2. For some topologies, several materials have been tested. In some cases, the use of several samples was necessitated by the sparse amount of each sample, while in other cases, several samples were tested and compared in order to elucidate whether the observed axial deactivation pattern is a general feature of the zeolite topology studied, or specific for one sample. In each case, focus will be set on the axial deactivation profiles observed. Differences in the overall activity and deactivation rates between materials

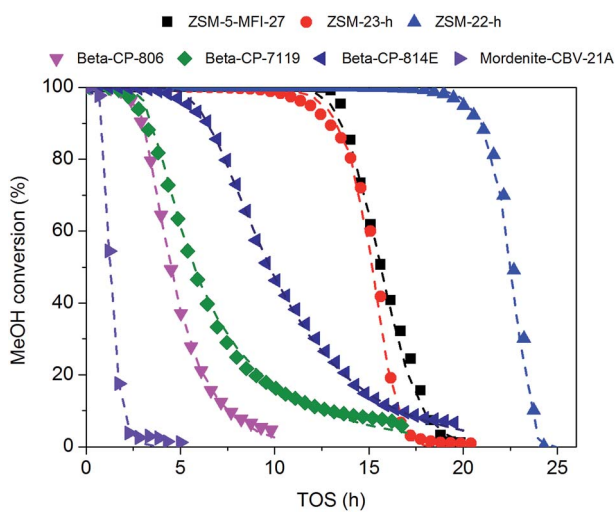

Fig. 1 Methanol conversion *versus* time-on-stream at 400 °C over the various catalysts tested. Experimentally measured data are represented by symbols while simulated deactivation curves are represented by dashed lines. $\tau_0 = 4$ g h^{-1} mol^{-1} was applied over ZSM-22-h and ZSM-23-h whereas for the rest of the catalysts $\tau_0 = 2$ g h mol^{-1} was used.

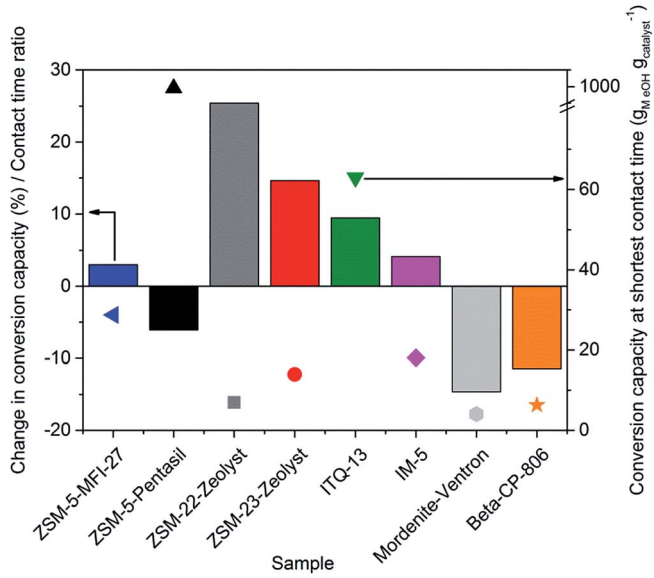

Fig. 2 Normalized variation of the methanol conversion capacity with respect to the increase in contact time on the different zeolites investigated (left axis). Methanol conversion capacity (g MeOH/g catalyst) of the different zeolites investigated at the shortest contact time (τ_0) (right axis).

belonging to the same topology, but with different morphology, acid site density or various lattice defects, have been the subject of previous reports and will not be discussed here.

3.1 Deactivation of ZSM-5 (MFI topology)

ZSM-5 is used in industrial MTG and MTP processes, and has been studied extensively over the past 40 years. It is therefore a natural starting point for this study. Two ZSM-5 catalysts were studied here, ZSM-5-pentasil and ZSM-5-MFI-27. Only ZSM-5-MFI-27 was tested until full deactivation.

As a first remark, the methanol conversion *versus* time on stream curve obtained over ZSM-5-MFI-27 (Fig. 1) displays an inverse sigmoidal shape with a rapid

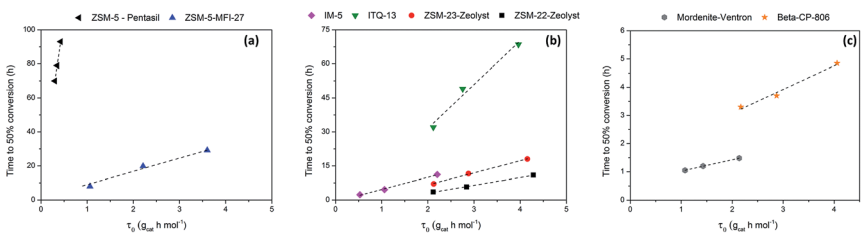

Fig. 3 Catalyst lifetime to 50% MeOH conversion ($t_{0.5}$) as a function of the applied contact time, τ_0 (weight to flow ratio W/F) on (a) ZSM-5-pentasil and ZSM-5-MFI-27, (b) IM-5, ITQ-13, ZSM-22-Zeolyst and ZSM-23-Zeolyst and (c) mordenite-Ventron and beta CP-806. The dotted lines are added as a guide for the eye.

Table 1 Calculated values of the critical contact times (τ_{crit}) and deactivation coefficients (a) using the autocatalytic deactivation model[a]

Sample	τ_{crit} (g h mol^{-1})	a (g mol^{-1})
ZSM-5-pentasil	0	0.004
ZSM-5-MFI-27	0	0.13
IM-5	0.14	0.19
ITQ-13	0.36	0.052
ZSM-22-Zeolyst	1.1	0.29
ZSM-23-Zeolyst	0.76	0.24
Mordenite-Ventron	*	2.5
Beta-CP806	*	1.2

[a] *Model not applicable, see bulk text.

decline in conversion after the breakthrough of methanol, followed by a flattening of the curve at less than 40% conversion. Numerous previous studies of ZSM-5 catalysts have shown the same conversion *versus* time-on-stream behaviour (see *e.g.* ref. 4, 12, 14, 16 and 29), which is typical for systems where the reactant is involved in coke formation.[2,42] Fig. S.1 (ESI†) shows the product yield of ZSM-5-MFI-27 with respect to time on stream. In agreement with previous studies, the product stream consists mainly of C_2–C_5 alkenes, as well as arenes and paraffins.[29,34]

The methanol conversion capacity ($g_{MeOH}\ g_{cat}^{-1}$) of the two ZSM-5 samples is only moderately influenced by the applied contact time (Fig. 2). For ZSM-5-MFI-27, a slight increase in conversion capacity with longer contact time is observed,

Table 2 Summary of the characterization results of the fresh catalysts

Sample	Si/Al ratio	BET surface area ($m^2\ g^{-1}$)	External area ($m^2\ g^{-1}$)	Total pore volume ($cm^3\ g^{-1}$)	Micropore volume[a] ($cm^3\ g^{-1}$)	Particle size (μm)	$\Delta\nu$ ((OH) cm^{-1}) upon CO adsorption
IM-5	15	482	118	0.81	0.15	0.2–1	313
ITQ-13	50	461	40	0.39	0.17	0.2–1	305
ZSM-22-Zeolyst	45	217	20	0.14	0.08	2–4	315
ZSM-23-Zeolyst	23	159	56	0.66	0.05	0.2–1	320
Mordenite-Ventron	11	573	44	0.40	0.22	0.2–1	310
ZSM-5-pentasil	45	422	113	0.61	0.14	0.05–0.1	313
ZSM-5-MFI-27	15	414	5	0.18	0.17	1–4	306
Beta-CP806	17	677	188	0.99	0.19	<0.1	311
Beta-CP-814E	14	653	248	1.05	0.16	<0.1	—
Beta-CP-7119	13	657	26	0.37	0.26	0.5	—
Mordenite-CBV-21A	11	525	27	0.26	0.19	0.1–0.3	—
ZSM-22-h	41	268	55	0.49	0.08	0.5–1	—
ZSM-23-h	28	222	45	0.26	0.07	0.5–1	—

[a] *t*-Plot.

in line with the results reported by Bleken.[29] In that study, a 10% increase in methanol conversion capacity was observed upon a ten-fold increase in contact time over a ZSM-5 catalyst. For ZSM-5-pentasil, a minor decrease in the methanol conversion capacity is observed with increasing contact time (Fig. 2). This discrepancy could be due to an extrapolation uncertainty because the cumulative conversion for ZSM-5-pentasil was extrapolated when the conversion of methanol was still at 10%.

As shown in Fig. 3, the $t_{1/2}$ values for ZSM-5-pentasil obtained at τ_0 between 0.30 and 0.43 g h mol^{-1} are considerably higher than those of ZSM-5-MFI-27, obtained at τ_0 between 1.1 and 3.6 g h mol^{-1}. Variations in the catalyst lifetime between the two ZSM-5 samples are attributed to the differences in their Si/Al ratio and crystal size (Table 2), in accordance with previous studies.[43,44]

In line with previously reported results over ZSM-5,[12] the $t_{1/2}$ *versus* τ_0 curves for ZSM-5-pentasil and ZSM-5-MFI-27 cross the *x*-axis very close to the origin (Fig. 3). In other words, τ_{crit} can be considered negligible and consequently, the auto-catalytic reaction dominates in ZSM-5 regardless of the applied contact time.

The value of the deactivation constant (*a*) (see Table 1) in ZSM-5-MFI-27 far exceeds that of ZSM-5-pentasil, in line with the higher conversion capacity of ZSM-5-pentasil obtained by integrating the conversion *versus* time on stream curves (Fig. 2). Indeed, the deactivation constant in the latter material is the lowest among all the tested zeolites (*vide infra*), reflecting its superior catalyst stability.

For the spatio-temporal study, four individual tests were carried out using ZSM-5-MFI-27 at a constant $\tau_0 = 2$ g h mol^{-1}. The reaction was quenched after 5, 10, 15 and 20 hours on stream, when the methanol conversion was 100%, 100%, 80% and 0%, respectively (Fig. 1). Photographs of the catalyst bed after each test are shown in Fig. 4, top. A color gradient was observed along the catalyst bed, in particular after 5 and 10 hours on stream, *i.e.* before methanol breakthrough (Fig. 1).

The dark first layers of the catalyst bed display evidence of a more deactivated region, whereas the light grey color of the lower part of the bed suggests that this region is deactivated to a lesser extent.

The BET surface area and the total amount of coke determined by TG analysis in the four catalyst layers obtained after each time on stream are shown in Fig. 4, bottom. Concerning the spatial distribution of coke along the bed, after the 5 and 10 hour experiments, thermogravimetric analysis unequivocally shows that there is a substantial decrease in the total amount of oxidizable coke species when moving from the entrance towards the outlet of the catalyst bed. Besides, the BET area is strongly reduced in the top (entrance) layer owing to the amount of coke deposited in this fraction, while it is gradually less reduced in the bottom layers of the bed.

During the first 10 hours of reaction, the product distribution (Fig. S.1 ESI†) is independent of coke deposition, in agreement with previous studies,[11,29,45] and only after the breakthrough of methanol, the product distribution as well as the evolution of coke and BET area change. The large gradient in coke content observed during the first 10 hours of reaction was reduced for the 15 h experiment, where still a minor difference between the top and bottom layers is observed due to the residual activity of the bottom-most catalyst layer. However in the completely deactivated sample (20 h on stream), the differences in the coke

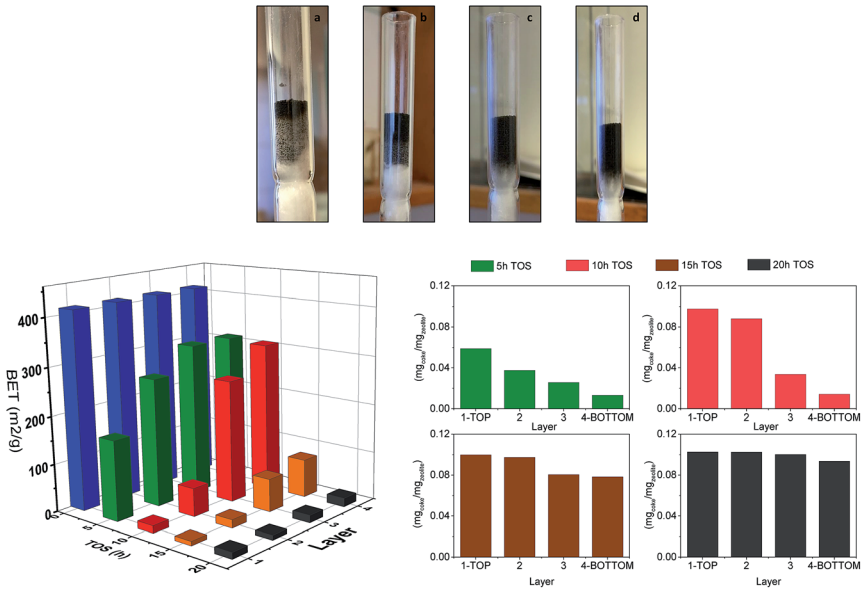

Fig. 4 Top: ZSM-5-MFI-27 deactivated at $t = 5$, 10, 15, and 20 hours (a, b, c and d, respectively) in the 9 mm reactor, $T = 400$ °C, $\tau = 2$ g h mol^{-1}. Bottom-left: BET area on partially deactivated catalyst layers of ZSM-5. Bottom-right: Normalized amounts of total coke in the different fractions of ZSM-5-MFI-27.

amount and BET area along the catalyst bed are negligible. These data are in line with previous studies of ZSM-5 catalysts.[9,13,14,19,46]

Different from the previously reported results,[29] no white layer was observed at the entrance of the catalyst bed. The first layer shows the most profound deactivation. Such discrepancy can be attributed to the different experimental conditions used. Bleken[29] used shorter contact times ($\tau = 0.05$–0.48 g h mol^{-1}). With such low contact times, even for ZSM-5, an initiation zone for the build-up of the autocatalytic species (and coke) was observed.

In order to get further insight into the distribution of coke along the bed, soluble coke species trapped in the pores were analyzed following the Guisnet protocol[40] in the four segments of ZSM-5-MFI-27. The data are reported in Fig. S.8 in the ESI.†

The distribution of soluble coke species agrees well with the TG data. Soluble species were only detected in the top layers of the catalyst bed. For the 5 and 10 hour experiments, in the bottom-most layers, no retained soluble species were extracted. It is only after the breakthrough of methanol that soluble coke species are identified in these layers. This result further confirms that the deactivation front is moving downwards along the bed and, although insoluble coke was observed in the lower fractions of the bed, it is only the fractions where methanol is present that contain soluble coke species. Finally, it should be noted that no changes were observed in the species identified at increasing times on stream. This can be interpreted as an accumulation of the same type of deactivating species throughout the bed, and/or to a steady-state situation of formation and further conversion of such species to insoluble coke.

The results obtained in this section show full agreement between the two catalysts and test methods used, and with previous studies of ZSM-5 catalysts, *i.e.* that methanol is a main source of catalyst deactivation in this topology,[29] either *via* formaldehyde (reaction (1)) or by reaction between methanol and hydrocarbon products (reaction (2)), with a smaller contribution of coke formation from products alone (reaction (3)).

3.2 Deactivation of ZSM-22 (TON topology)

Two ZSM-22 materials were tested in this contribution: the commercial ZSM-22-Zeolyst was used in studies of catalyst deactivation and methanol conversion capacity *versus* applied contact time, while the home-made ZSM-22-h was used in the spatio-temporal study. The conversion *versus* time on stream curve for ZSM-22-h is shown in Fig. 1 and has a similar shape to that observed for ZSM-5, with rapid deactivation after methanol breakthrough, albeit much less flattening of the curve at low conversion. Furthermore, differently from ZSM-5, the conversion capacity of ZSM-22-Zeolyst increases significantly with an increase in contact time (Fig. 2). Such an increase has previously been reported for ZSM-22 by Teketel *et al.*[15] and Janssens *et al.*[12]

The product yield obtained over ZSM-22-h is shown in Fig. S.2 (ESI†). In agreement with previous studies of ZSM-22,[10,15] an alkene rich product spectrum is obtained with near complete absence of aromatics.

Plots of $t_{1/2}$ *versus* contact time for ZSM-22-Zeolyst are shown in Fig. 3 (middle panel). Extrapolation of the curve to $t_{1/2} = 0$ displays a substantial initiation zone in these experiments, the critical contact time being 1.1 g h mol^{-1}, *i.e.* 25–50% of the applied contact time, τ_0, in these experiments. This observation complements the higher methanol conversion capacity of this material with increasing contact times, obtained by integrating the conversion *versus* time on stream curves until full deactivation (Fig. 2). Thereby, the applicability of the autocatalytic deactivation model for this catalyst topology is confirmed.

The deactivation constant ($a = 0.292$ g mol^{-1}, see Table 1) in ZSM-22-Zeolyst reflects its limited catalyst stability in the MTH process, in line with previous studies where its conversion capacity was found to be comparable to that of the commercial MTO catalyst, SAPO-34.[15]

The deactivation in ZSM-22-h was spatially and temporally investigated at 400 °C and at a constant contact time ($\tau_0 = 4$ g h^{-1} mol^{-1}). Fig. 5 shows the evolution of coke and BET area for the catalyst layers obtained at increasing reaction times. The MTH reaction over ZSM-22-h was quenched at 5, 15, 21 and 24 hours on stream, corresponding to 100%, 100%, 90% and 0% methanol conversion (Fig. 1).

The deactivation pattern obtained in ZSM-22-h is comparable to that previously shown for ZSM-5. During the early stages of reaction, the catalyst layer closest to the reactor entrance suffers from a higher degree of deactivation *i.e.* larger reduction in BET area and higher accumulation of coke, compared to the subsequent catalyst layers. At longer reaction times, particularly after the methanol breakthrough, the differences in terms of coke content and BET surface area are minimised among the layers of ZSM-22-h, suggesting that the catalyst bed is deactivated to a similar extent.

It is important to note that the ZSM-22 (and ZSM-23, *vide infra*) catalysts used for the contact time influence tests are different from the samples used in the

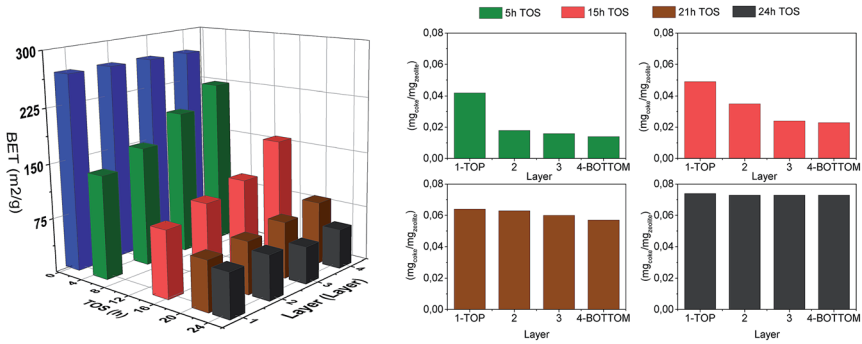

Fig. 5 Evolution of BET surface area (left) and total coke content obtained by TG (right) on ZSM-22-h at increasing reaction times.

spatiotemporal investigation, due to limited amounts of each material. In the former case commercial samples from Zeolyst were used, but in the latter, samples were synthesized in house. The catalyst lifetime of the in-house synthesized ZSM-22 shows a longer lifetime than previously reported results on ZSM-22.[15,47,48] The improvement in the catalyst lifetime of this particular sample warrants further studies.

Since the initiation zone fraction of the ZSM-22-h catalyst bed is unknown, it is of particular relevance for this study that del Campo *et al.* recently studied the deactivation of ZSM-22-Zeolyst using space- and time-resolved operando X-ray diffraction with the same contact time and slightly lower temperature (375 °C) compared to the current study.[48] Rapid deactivation (methanol breakthrough), starting immediately after the onset of the experiment, was observed. Furthermore, the unit cell expansion in the ZSM-22-Zeolyst due to the formation of coke species was invariant throughout the bed, for the duration of the test. In the same study, an acid–base treated ZSM-22-Zeolyst catalyst, with improved methanol conversion capacity compared to the parent material, was tested. Over that catalyst, the cell expansion was more rapid in the first layers of the catalyst bed compared to the subsequent catalyst layers, suggesting more rapid deactivation of the first layer of the catalyst bed, in agreement with the results obtained for ZSM-22-h in this study.

Together, current and previous studies of ZSM-22 suggest that methanol is a main source of coke formation in this topology, with substantially lower contribution of coke formation from product–product reactions. Further evidence of such a conclusion is found in a recent study by Teketel *et al.*, who observed an increasing methanol conversion capacity over ZSM-22 when co-feeding methanol with propanol or butanol. The co-feeding of these higher alcohols (which dehydrate under reaction conditions into the corresponding alkenes) led to an increase in the methanol conversion capacity by 4- or 5-fold when co-feeding propanol and butanol, respectively, in comparison with a pure methanol feed.[49]

3.3 Deactivation of ZSM-23 (MTT topology)

The ZSM-23 topology was tested at applied contact times, τ_0, between 2–4 g h mol^{-1}, using two samples; ZSM-23-Zeolyst (contact time variation) and ZSM-23-h

(spatio-temporal study). Characterization data for the two samples are shown in Table 2. The conversion of methanol *versus* time on stream to complete deactivation with a contact time $\tau_0 = 4$ g h mol^{-1} is shown for the ZSM-23-h sample in Fig. 1. Its deactivation pattern was very similar to that of ZSM-22, with rapid deactivation after methanol breakthrough, and little flattening at low conversion. Product distribution *versus* time on stream and methanol conversion plots are shown in Fig. S.3† and displays similarities to the product distribution obtained over ZSM-22, with propene and C_{5+} alkenes as main products and without noticeable amounts of aromatic compounds, as it has been previously reported.[30]

An increase in the contact time resulted in a higher methanol conversion capacity for the ZSM-23-Zeolyst, as it was also observed for the ZSM-22-Zeolyst (Fig. 2). Such an increase has also previously been reported for this topology.[30]

A plot of $t_{1/2}$ *versus* applied contact time, τ_0, for this topology showed a substantial critical contact time before onset of the autocatalytic reaction (Fig. 3), *i.e.*; $\tau_{crit} = 0.76$ g h mol^{-1} with a deactivation constant $a = 0.242$ g mol^{-1} (Table 1). In accordance with the evolution of the conversion capacity at increasing contact times (Fig. 2), τ_{crit} was lower for ZSM-23-Zeolyst than for ZSM-22-Zeolyst. According to the autocatalytic deactivation model, such a result suggests that the initiation zone of this catalyst is non negligible, different from ZSM-5 and similar to ZSM-22, and furthermore, that the first zone of the catalyst bed has negligible activity in the autocatalytic MTH reaction.

For the spatiotemporal study of ZSM-23-h deactivation, a constant contact time $\tau_0 = 4$ g h mol^{-1} was used. The evolution of the BET area and coke content on the partially spent layers of the catalyst is shown in Fig. 6. A similar deactivation pattern to that obtained in ZSM-5 and ZSM-22 was observed for ZSM-23-h. For this material, the MTH reaction was quenched at the very beginning of the reaction after only 20 minutes, and after 5, 10, and 19 hours, corresponding to 100%, 100%, 98% and 0% methanol conversion, respectively (Fig. 1).

Even for the shortest experiment (20 minutes on stream), the topmost layer displays a darker color in comparison to the rest of the bed. Regarding the evolution of the BET surface area and the amount of coke, the first layers show a larger decrease of the BET area and a higher amount of coke than the layers located towards the outlet of the bed.

It is worth highlighting the rapid accumulation of coke in the first layer of the ZSM-23 catalyst bed. After only 20 minutes under reaction conditions, the total coke content in this topmost layer reaches 78% of the coke detected in the completely deactivated sample. The combination of a substantial initiation zone and a rapid deactivation of the first catalyst layer even at the shortest contact time could suggest that methanol is the main source of coke formation, and that the initial selectivity of methanol conversion *via* formaldehyde (reaction (1)) favors coke formation over the formation of autocatalytic species (*vide infra*).

3.4 Deactivation of IM-5 and ITQ-13 (IMT and ITH topology)

IM-5 and ITQ-13 were subjected to deactivation *versus* applied contact time studies, but not to spatio-temporal investigations. Both materials displayed

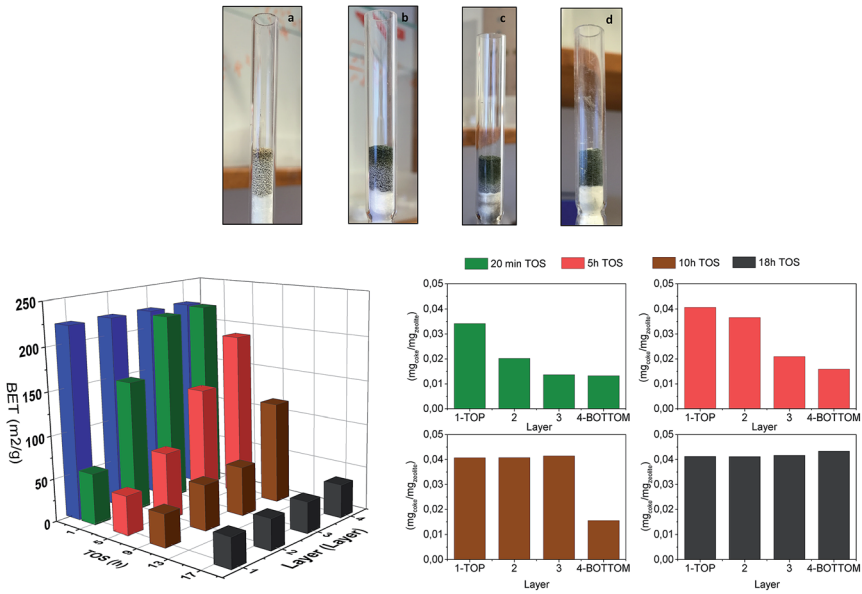

Fig. 6 Top: Photos of ZSM-23-h after quenching the reaction at (a) 20 minutes, (b) 5, (c) 10 and (d) 19 hours on stream, $T = 400$ °C, $\tau_0 = 4$ g h^{-1} mol^{-1}. Bottom-left: BET area on the partially deactivated catalyst layers of ZSM-23. Bottom-right: Normalized total coke content in ZSM-23.

a similar response to contact time variations as the 1D 10-ring topologies ZSM-22 and -23 with an increase in the methanol conversion capacity with increasing applied contact time (Fig. 2), matched by a significant critical contact time (0.14 g h mol^{-1} for IM-5, 0.36 g h mol^{-1} for ITQ-13; Fig. 3 and Table 1) which was, however, substantially shorter than for the ZSM-22 and -23 (Table 1). The deactivation constant of IM-5 (0.186 g mol^{-1}) was slightly lower than for ZSM-22 and -23, while it was much lower for ITQ-13 (0.052 g mol^{-1}, Table 1). Overall, the deactivation of these two topologies was intermediate between the 3D 10-ring ZSM-5 topology, and the more narrow-pored 1D 10-ring ZSM-22 and -23 topologies, in agreement with their intermediate pore dimensionality and size.

3.5 Deactivation of beta zeolite (BEA topology)

To the best of our knowledge, no spatio-temporal study of 12-ring zeolites for the MTH reaction has been published before. Therefore, three samples with BEA topology were subjected to spatio-temporal studies in this contribution: beta-CP-806, beta-CP-7119 and beta-CP-814E, while one sample, beta-CP-806, was subjected to applied contact time variation studies. Conversion *versus* time on stream curves for the three samples are shown in Fig. 1. Their shape is similar to one another, but is markedly different from those of the 10-ring topologies, with a rather fast breakthrough of methanol, followed by a deactivation curve for which the slope decreases with the progress of catalyst deactivation. The product selectivity over beta-CP-806 (Fig. S.4†) is dominated by aromatic compounds,

followed by butenes and branched C_{5+} species, in agreement with previous studies.[50,51]

Distinct differences between 12-ring and 10-ring topologies are also observed in the tests with varying applied contact times. A decrease in the conversion capacity with increasing contact time is observed for beta-CP-806 (Fig. 2), which is opposite to the trend observed in the medium pore size zeolites (except for ZSM-5). Furthermore, in spite of the linear dependency of $t_{1/2}$ on τ_0 in the experiments performed at different contact times (Fig. 3), results of the deactivation constant (a) and τ_{crit} (Table 1) are markedly different from those observed for the medium pore size zeolites. Interestingly, a negative value is obtained for the critical contact time over beta-CP-806. This result lacks a physical meaning, since according to the autocatalytic deactivation model, it would mean that even without feeding methanol the autocatalytic reaction is dominating. While this observation evidences the shortcoming of the autocatalytic model for the beta topology, the observation of a decrease in the methanol conversion capacity with increasing applied contact time might be explained by an increase in secondary reactions between the hydrocarbon products in the large pore beta topology (Rx. (3)), leading ultimately to the experimentally observed faster coking, and as a consequence a decrease in methanol conversion capacity with a larger product zone (*i.e.* increasing contact time). It is natural to correlate the enhanced influence of product–product reactions leading to coke formation in this topology, to the large pore size of 12-ring zeolites, which facilitates the diffusion of large product molecules into the zeolite pores, even in the product zone of the catalyst bed.

The deactivation in beta-CP-806 was also investigated spatially and temporally resolved, using the same reaction conditions as for ZSM-5-MFI-27 (400 °C and $\tau_0 = 2$ g h^{-1} mol^{-1}). The MTH reaction over beta-CP-806 was quenched at 1, 3, 5 and 10 hours on stream, corresponding to 100%, 90%, 35% and 3% methanol conversion (Fig. 1).

The obtained deactivation pattern along the catalyst bed of beta-CP-806 was very different from that observed in medium pore size zeolites.

Fig. 7 shows the total coke content and the BET surface area of the partially deactivated layers of beta-CP-806. The first remarkable difference with respect to the 10-ring zeolites is the visual aspect of the catalyst bed. Even for the shortest reaction time (1 hour on stream and full methanol conversion), the catalyst bed is completely black without any axial gradient in color along the bed. Moreover, no significant difference in the reduction of BET area compared to the fresh sample were observed between the catalyst layers, again suggesting that they are equally deactivated (Fig. 7, blue bars). With increasing time on stream the degree of reduction of BET area compared to the parent material increases; and again, the deactivation seems to be homogeneous along the bed. Thermogravimetric analyses also show that coke is evenly distributed throughout the segments of catalysts in contrast to the clear gradients observed in ZSM-5, ZSM-22 and ZSM-23.

In order to get further insight into the distribution of coke along the bed, soluble coke species trapped in the pores were analyzed following the Guisnet protocol[40] in the deactivated segments of beta-CP-806. Fig. S.9 in the ESI† shows the chromatograms of the soluble coke species extracted in beta-CP-806. Clearly, soluble species are homogeneously distributed along the catalyst layers, even

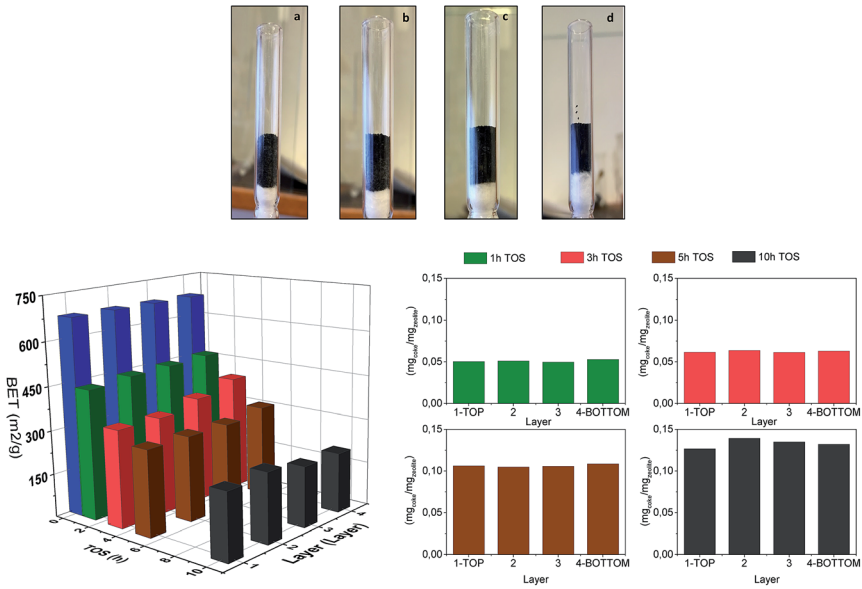

Fig. 7 Top: Photos of beta CP-806 after quenching the reaction at (a) 1 h, (b) 3 h, (c) 5 h and (d) 10 hours on stream. Bottom: Evolution of BET area (left) and normalized total coke content (right) in the layers of beta-CP-806 at increasing times on stream.

before the breakthrough of methanol, again suggesting that hydrocarbon products are strongly involved in coke formation. Finally, at increasing TOS, a decrease in the amount of soluble species is observed, together with a shift towards heavier and more thermodynamically favored species, in line with previous studies carried out over beta zeolites.[25] These results again confirm the different deactivation patterns of 10- and 12-ring topologies. Moreover, the amount of soluble species detected in the large beta-CP-806 is significantly lower than that in ZSM-5-MFI (note the differences in scale of Fig. S.8 and S.9†), suggesting rapid conversion of these species to insoluble coke species in the more spacious BEA pores.

Another difference between beta-CP-806 and the 10-ring topologies is that the product yield over beta-CP-806 is not independent of the coke content before the breakthrough of methanol (Fig. S.5 in the ESI†). Instead, the C_{5+} fraction increases at the expense of the C_4 products with increasing TOS, and reaches a maximum before the breakthrough of methanol.

In order to investigate whether the observed deactivation pattern is a general feature of the BEA topology, two additional beta samples were studied. Both beta-CP-814E (Fig. 8) and beta-CP-7119 (Fig. S.6†) show a very similar axial deactivation pattern to that observed in beta-CP-806: a uniform decrease in the BET surface area accompanied by an even accumulation of coke is observed for the different segments of the catalyst bed quenched at the same time on stream.

These results demonstrate that the observed axial deactivation pattern is not affected by the selection of the sample. Rather, it is a general pattern for samples with BEA topology.

3.6 Deactivation in mordenite (MOR topology)

Two mordenite samples were studied; mordenite-CBV-21A was used in the spatio-temporal studies, while mordenite-Ventron was used in the applied contact time variation studies. The conversion *versus* time on stream plot at 400 °C and $\tau_0 = 2$ g h mol^{-1} of mordenite-CBV-21A is shown in Fig. 1. A very rapid deactivation is observed, followed by a flattening of the curve close to full deactivation. The product yield is shown in Fig. S.7† and it shows a high initial yield of lower olefins with noticeable amounts of methane in the effluent at short reaction times, in line with previously reported results.[52]

A decrease in methanol conversion capacity with increasing contact time was observed for mordenite-Ventron, similar to the beta-CP-806 sample (Fig. 2). Furthermore, a linear correlation between applied contact time and $t_{1/2}$ was observed (Fig. 3), enabling the calculation of critical contact time and deactivation rate by the autocatalytic model. However, as for beta-CP-806, a negative critical contact time was obtained, indicating the failure of the autocatalytic deactivation model to correctly describe the deactivation of the MOR topology. Again, we hypothesize that the origin of these observations is due to a dominance of secondary reactions between hydrocarbon products that transform into coke, compared to coke originating from methanol.

Concentrating next on the spatio-temporal study of mordenite-CBV-21A (Fig. 9), the reaction was quenched after 20, 35, and 70 minutes, and 5 hours on stream, corresponding to 100%, 100%, 55% and 0% methanol conversion, respectively. The axial pattern is similar to what is observed for the beta samples: the coke content and BET surface area of each catalyst layer is similar throughout the bed at all times on stream investigated.

4. Discussion

The zeolite topologies studied in this contribution span a wide range of MTH catalysts, from a 1D 10-ring topology with high C_{5+} alkene selectivity, where alkenes are the autocatalytic engines and even monocyclic aromatic compounds are retained as inactive coke species in the pores (ZSM-22)[15,30] *via* a 3D 10-ring

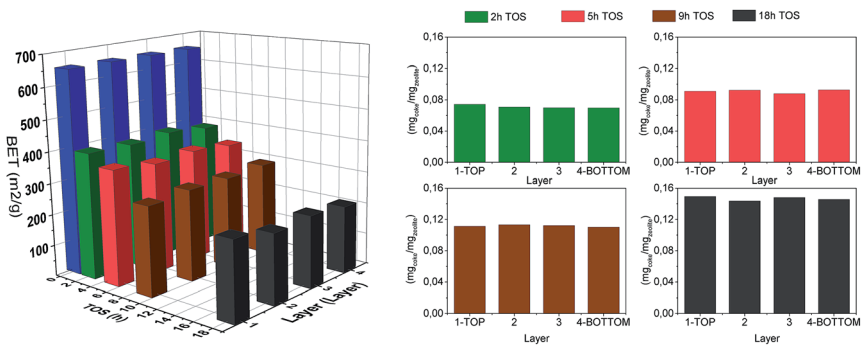

Fig. 8 Evolution of BET surface area (left) and coke content (right) on the partially deactivated layers of beta CP-814E

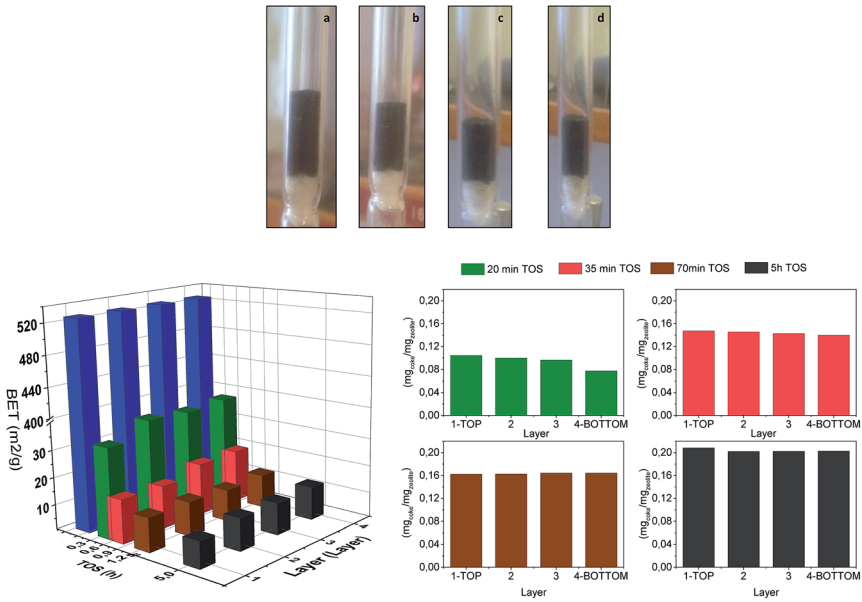

Fig. 9 Top: Visual evidence of the catalyst bed of mordenite CBV-21-A after quenching the reaction at (a) 20 min, (b) 35 min, (c) 70 min and (d) 5 hours on stream. Bottom: BET surface area (left) and coke content (right) on the partially deactivated layers of CBV-21-A at increasing TOS.

topology where alkenes and arenes work together as autocatalytic engines and where the effluent products are distributed between light alkenes, alkanes and arenes up to C_{10} (ZSM-5),[5,29] to a 3D 12-ring topology where light alkanes, alkenes and arenes up to C_{12} are the main products and where arenes together with alkenes are the dominating autocatalytic engines (beta).[50,51]

Among the 7 topologies studied, only two (ZSM-5 and ZSM-22) have previously been subjected to systematic studies of axial catalyst deactivation patterns. Hence, the systematic study reported herein fills the gap in pore size and dimensionality between those two topologies, and expands the parameter space to large-pore 12-ring zeolites.

4.1 Influence of catalyst topology on the origin and impact of coke formation

As a first general remark to the results reported in Section 3, current and previous studies of several samples belonging to the same topology demonstrate that the observed axial deactivation pattern is a general feature of each topology, and not limited to one particular sample. Considering next the origin of coke formation, *i.e.* methanol *versus* hydrocarbon products, the impact of hydrocarbons alone as coke precursors can quite straightforwardly be assessed from the spatio-temporal studies, in particular the coke amounts formed in the product zone compared to that formed in the initiation and autocatalytic zones. As such, a clear correlation is observed between zeolite topology and the axial deactivation pattern (Fig. 4–9): the larger the pore size, the more important the

influence of coke formed from the conversion of hydrocarbon products. Conversely, the smaller the pore size, the more important the formation of coke from methanol. As mentioned above, the distinction between 10-ring and 12-ring topologies with respect to coke formation from hydrocarbon products alone is likely related to the facile diffusion of product molecules in and out of large-pore zeolites.

Considering next the coke formation from methanol alone, *i.e. via* formaldehyde (reaction (1)), compared to coke formation from methanol and hydrocarbons (reaction (2)), the correlation is less straightforward, in particular for topologies such as ZSM-5, beta, and mordenite, where no critical contact time is observed in the contact time variation experiments (Fig. 3). However, the ensemble of test data obtained for 10-ring zeolites with more narrow pore size than ZSM-5 show a substantial initiation zone, combined with coke formation in the top layer of the catalyst bed (Fig. 2, 5 and 6), and therefore strongly suggest that reaction (1) contributes to coke formation. One additional parameter may help to further clarify the relative impact of reactions (1) and (2): methane formation. If coke is formed exclusively *via* formaldehyde (Rx. (1)), then the cumulative mass of methane formed in the experiment should be similar to the cumulative mass of coke. If coke is formed from reactions between methanol and hydrocarbons (which could likely be secondary products from Rx. (1)), then the hydrogen abstraction required to subsequently form (poly-)aromatic and graphitic species could proceed by hydrogen transfer either to methanol (thereby forming methane) or to a hydrocarbon such as an alkene (thereby forming the corresponding alkane). The commonly reported correlation between the hydrogen transfer index (HTI), (*i.e.* the alkane fraction in aliphatic products), and the aromatics fraction in the effluent could suggest that hydrogen transfer to another hydrocarbon is the most common mechanism of hydrogen abstraction.[33] In this respect, it is of interest to note that for the ZSM-23 catalyst, where rapid coke accumulation was observed in the first catalyst layer during the first 20 minutes on stream, the total amount of CH_4 formed during those first 20 minutes was 0.5 mg CH_4 per $g_{catalyst}$, whereas the coke content in the first layer of ZSM-23 was 34 $mg_{coke}\ g_{catalyst}^{-1}$, *i.e.* close to two orders of magnitude higher. This result clearly suggests that reaction (1) mainly serves as an initiation reaction, which subsequently leads to coke formation by interactions between methanol and hydrocarbons.

Considering finally the overall performance of the various topologies with respect to conversion capacities (Fig. 2) and deactivation rates (Table 3), the ensemble of data should be considered with care due to the different Si/Al ratios and crystal sizes of the individual samples (Table 2). However, as a general trend, it is interesting to note that the 12-ring topologies have limited conversion capacity due to their high deactivation rates, while the conversion capacity of 10-ring topologies is equally related to their substantial critical contact time.

4.2 A simplified model of catalyst deactivation

Spatio-temporal studies of catalyst deactivation may be experimentally challenging for large sample libraries. It is therefore of interest to elucidate whether

Table 3 Simulated rate constants of the reactions (6)–(8)

Sample	k_1	k_2	k_3
ZSM-5-MFI-27	19 315	63	26
ZSM-23-h	1420	98	0
ZSM-22-h	2368	108	0
Beta-CP-806	3202	41	72
Beta-CP-7119	3575	17	68
Beta-CP814-E	4526	21	42
Mordenite-CBV-21A	3166	72	87

the coke origin in a given test of an MTH catalyst may be hypothesized by visual inspection of the shape of the conversion *versus* time on stream curve. If so, one could easily assess whether or not the deactivation rate of various samples could be compared by applying the autocatalytic deactivation model (which is limited to tests where methanol is a main coke precursor (*vide infra*)).

Olsbye[7] recently suggested a simple model to distinguish between coke formation from reactants and products. In that model, all reaction rates are assumed to be first order in the reacting molecule. Methanol, A, is the reactant, B is the effluent product, C is the coke and N is the number of active sites.

$$\mathrm{A} \xrightarrow{k_1} \mathrm{B} \qquad -\mathrm{d[A]}/\mathrm{d}t = (k_1 + k_2)[\mathrm{A}]N \tag{6}$$

$$\mathrm{A} \xrightarrow{k_2} \mathrm{C} \quad \mathrm{d[C]}_i/\mathrm{d}t = (k_2[\mathrm{A}] + k_3[\mathrm{B}])N \tag{7}$$

$$\mathrm{B} \xrightarrow{k_3} \mathrm{C} \quad \mathrm{d[B]}/\mathrm{d}t = (k_1[\mathrm{A}] - k_3[\mathrm{B}])N \tag{8}$$

In the current contribution, this simple model has been used to determine the rate constants k_1, k_2 and k_3 for each of the tests reported in Fig. 1, by regression analysis. The reactor was modelled as a series of 21 segments (9 in the case of MOR), where each segment was considered a CSTR reactor. The concentrations of A, B and C were integrated along the catalyst bed for each time on stream. Furthermore, the total coke content, C, and change in number of active sites, N, in each segment (i) was integrated with time on stream (j).

$$N_{i,j} = N_{i,j-1} - C_{i,j} \tag{9}$$

Fig. 1 depicts the experimental (symbols) and the simulated (dashed line) conversion curves *versus* time on stream over the samples used in the spatio-temporal study. The simulated rate constants are reported in Table 3.

As a first comment to the data in Table 3, the rate constant of the main reaction (k_1) clearly surpasses the value k_2 and k_3 in all the catalysts, as expected. Furthermore, the relative values of the two latter constants correlate with the shape of the deactivation curves, as follows.

First, the experimental MeOH conversion curves obtained for ZSM-5, ZSM-22 and ZSM-23 take an inverse S form with a rapid drop in conversion after the breakthrough of methanol. In the three medium-pore size zeolites, the rate

constant corresponding to the formation of coke from the reactants (k_2) is larger than k_3, assigned to the formation of coke from the products of the reaction. In particular, for ZSM-22 and ZSM-23, where the flattening of the conversion *versus* time on stream curve is less pronounced than for ZSM-5, the model provides a value equal to 0 for k_3. This can be interpreted as if coke in these rather narrow-pore 10-ring zeolites originates exclusively from reactions involving methanol. In ZSM-5, the value of k_2 is more than two-fold of the value of k_3, suggesting that methanol is a main source of coke formation also in this case, however, with a significant contribution of coke formed from hydrocarbon products.

Second, the three beta zeolites show a deactivation curve for which the slope decreases with time on stream, as the product concentration decreases. In these 3D-12 ring zeolites, the value of k_3 is at least two-fold that of k_2, suggesting that coke is formed to a larger extent from the products of reaction.

Finally, mordenite-CBV-21A shows an intermediate situation where a rapid decline in conversion is observed after methanol breakthrough but where the slope of the curve decreases at low conversion. The calculated rate constants indicate that the formation of coke is due to both reactants and products but the latter contribute somewhat more to the formation of coke.

In conclusion, a clear correlation is observed between this simple model and the results reported in the spatio-temporal studies, suggesting that the shape of conversion *versus* time on stream curves is a valuable indicator of coke formation patterns in the catalyst bed.

4.3 Influence of catalyst topology on critical contact time

Finally, another particularly interesting observation of this study is the increase in critical contact time, *i.e.* the contact time needed to launch the autocatalytic reaction, with a decrease in pore size for the 10-ring zeolites. The critical contact time is particularly long for the 1D 10-ring materials, ZSM-22 and -23, shorter for IM-5 and ITQ-13, and negligible for ZSM-5, beta, and mordenite. In all cases, substantial coke formation is observed in the first layer of the catalyst bed. This last observation suggests that methanol conversion is significant in the first layer of all topologies. However, in some topologies it leads mainly to coke formation and only to a small fraction of hydrocarbon pool species, while in others it leads to substantial formation of hydrocarbon pool species and effluent products, alongside with coke.

We suspect that the reason for this difference is the distinct role played by polymethylated benzene (PMB) molecules in the different topologies. In ZSM-22, PMB are inert coke molecules which are trapped in the pores.[15,30] In ZSM-5 and beta zeolite, however, PMB are hydrocarbon pool engines, and are also part of the effluent products[5,29,50,51]. In the intermediate structures between ZSM-22 and ZSM-5, IM-5 and ITQ-13, PMB are eluted as effluent products, but their possible role as hydrocarbon pool engines is yet to be revealed.

To elucidate the influence of PMB as effluent products, and PMB as hydrocarbon pool engines, on the observed critical contact time, two plots were made. In the first graph, (Fig. 10), the critical contact time is plotted *versus* effluent selectivity to aromatic products at 50% conversion. We considered this selectivity the most reliable measure of pore size under reaction conditions. In the

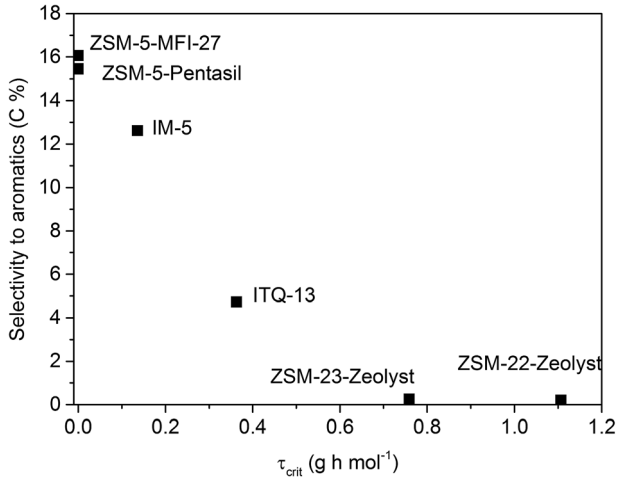

Fig. 10 Critical contact time (τ_{crit}) *versus* selectivity to aromatic products over medium pore size zeolites at 50% MeOH conversion.

second graph, the critical contact time is plotted *versus* the size of the largest sphere that can be inserted in the structure,[53] as a measure of cavity size (Fig. 11).

The plots show an inverse correlation between aromatics selectivity in the effluent and the critical contact time, whereas the correlation between the maximum cavity size and critical contact time is less evident. Based on this analysis, the ability of aromatic products to diffuse out of the zeolite crystals seems to be of primary importance for the rapid initiation of the autocatalytic MTH reaction.

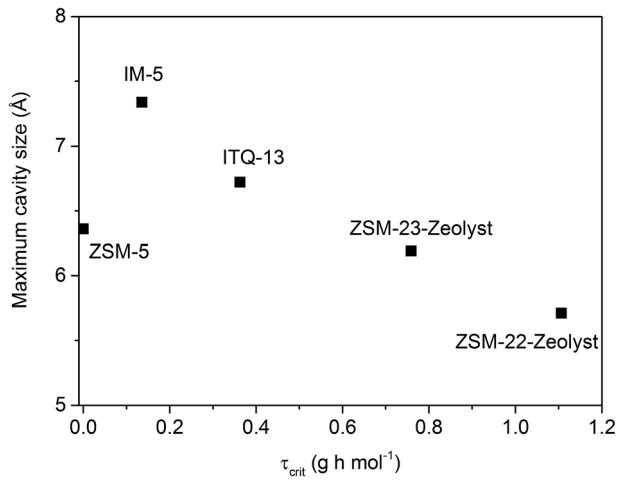

Fig. 11 Critical contact time (τ_{crit}) *versus* cavity size, measured as the largest sphere that can be inserted in the zeolite structure.

5. Conclusions

In this work we have examined the influence of zeolite topology on the axial mode of deactivation during the conversion of methanol to hydrocarbons. First, the autocatalytic deactivation model was used as a tool to determine the critical contact time and deactivation constant on seven different zeolites. The model was successfully applied in medium pore size topologies (ZSM-5, ZSM-22, ZSM-23, ITQ-13 and IM-5), yielding critical contact times and deactivation rates of each catalyst. In particular, it was found that the critical contact time increased with a decrease in pore size. Furthermore, the methanol conversion capacity of ZSM-5 varied little with contact time. However, the conversion capacity of the larger 12-ring topologies, mordenite and beta, decreased with an increase in contact time; in contrast to the 10-ring zeolites with pore sizes smaller than ZSM-5, for which the conversion capacity increased with an increase in contact time.

Furthermore, the deactivation on a selection of medium and large pore size zeolites has been investigated spatially and temporally. First, the catalyst bed was divided from top to bottom on increasingly deactivated samples. Secondly, the different layers of catalysts were characterized using nitrogen adsorption, thermogravimetric analysis and a dissolution–extraction protocol. The results revealed that zeolite topology affects not only catalyst lifetime and product distribution, but also modifies the axial mode of catalyst deactivation. Whereas the deactivation over medium pore size zeolites (ZSM-5, ZSM-22 and ZSM-23) occurs gradually from the entrance towards the outlet of the catalyst bed with gradients in the total coke content and evolution of BET area, in the case of beta and mordenite, the accumulation of coke and reduction of BET area in the larger pore size counterparts does not substantially vary along the catalyst bed layers, resulting in uniform deactivation throughout the catalyst bed.

Overall, this study has improved the understanding of the deactivation in the MTH process. Results show that the axial deactivation pattern and critical contact time change with zeolite topology, a concept which had not been addressed before.

Acknowledgements

This work is financially supported by the European Industrial Doctorates project "Zeomorph" (Grant Agreement No. 606965), as part of the Marie Curie actions (No. FP7-PEOPLE- 2013-ITN-EID). K. A. Lukaszuk and A. Molino are kindly acknowledged for the synthesis of ZSM-22-h and ZSM-23-h. Ms Sharmala Aravinthan is also acknowledged for her assistance with TG and N_2 adsorption experiments.

Notes and references

1 M. Stöcker, *Microporous Mesoporous Mater.*, 1999, **29**, 3–48.
2 U. Olsbye, S. Svelle, M. Bjørgen, P. Beato, T. V. W. Janssens, F. Joensen, S. Bordiga and K. P. Lillerud, *Angew. Chem., Int. Ed.*, 2012, **51**, 5810–5831.
3 B. Smit and T. L. M. Maesen, *Nature*, 2008, **451**, 671–678.
4 C. D. Chang and A. J. Silvestri, *J. Catal.*, 1977, **47**, 249–259.

5 M. Bjørgen, S. Svelle, F. Joensen, J. Nerlov, S. Kolboe, F. Bonino, L. Palumbo, S. Bordiga and U. Olsbye, *J. Catal.*, 2007, **249**, 195–207.
6 S. Svelle, F. Joensen, J. Nerlov, U. Olsbye, K. P. Lillerud, S. Kolboe and M. Bjørgen, *J. Am. Chem. Soc.*, 2006, **128**, 14770–14771.
7 U. Olsbye, S. Svelle, K. P. Lillerud, Z. H. Wei, Y. Y. Chen, J. F. Li, J. G. Wang and W. B. Fan, *Chem. Soc. Rev.*, 2015, **44**, 7155–7176.
8 M. Guisnet, L. Costa and F. R. Ribeiro, *J. Mol. Catal. A: Chem.*, 2009, **305**, 69–83.
9 H. Schulz, *Catal. Today*, 2010, **154**, 183–194.
10 S. Teketel, U. Olsbye, K.-P. Lillerud, P. Beato and S. Svelle, *Microporous Mesoporous Mater.*, 2010, **136**, 33–41.
11 T. V. W. Janssens, *J. Catal.*, 2009, **264**, 130–137.
12 T. V. W. Janssens, S. Svelle and U. Olsbye, *J. Catal.*, 2013, **308**, 122–130.
13 S. Müller, Y. Liu, M. Vishnuvarthan, X. Sun, A. C. van Veen, G. L. Haller, M. Sanchez-Sanchez and J. A. Lercher, *J. Catal.*, 2015, **325**, 48–59.
14 F. L. Bleken, K. Barbera, F. Bonino, U. Olsbye, K. P. Lillerud, S. Bordiga, P. Beato, T. V. W. Janssens and S. Svelle, *J. Catal.*, 2013, **307**, 62–73.
15 S. Teketel, S. Svelle, K.-P. Lillerud and U. Olsbye, *ChemCatChem*, 2009, **1**, 78–81.
16 F. Schmidt, C. Hoffmann, F. Giordanino, S. Bordiga, P. Simon, W. Carrillo-Cabrera and S. Kaskel, *J. Catal.*, 2013, **307**, 238–245.
17 D. M. Bibby, N. B. Milestone, J. E. Patterson and L. P. Aldridge, *J. Catal.*, 1986, **97**, 493–502.
18 P. L. Benito, A. G. Gayubo, A. T. Aguayo, M. Olazar and J. Bilbao, *Ind. Eng. Chem. Res.*, 1996, **35**, 3991–3998.
19 M. Kaarsholm, F. Joensen, J. Nerlov, R. Cenni, J. Chaouki and G. S. Patience, *Chem. Eng. Sci.*, 2007, **62**, 5527–5532.
20 J. Haw and D. Marcus, *Top. Catal.*, 2005, **34**, 41–48.
21 D. S. Wragg, M. G. O'Brien, F. L. Bleken, M. Di Michiel, U. Olsbye and H. Fjellvåg, *Angew.Chem., Int. Ed.*, 2012, **51**, 7956–7959.
22 M. Luo, H. Zang, B. Hu, B. Wang and G. Mao, *RSC Adv.*, 2016, **6**, 17651–17658.
23 X. Sun, S. Mueller, Y. Liu, H. Shi, G. L. Haller, M. Sanchez-Sanchez, A. C. van Veen and J. A. Lercher, *J. Catal.*, 2014, **317**, 185–197.
24 G. J. Hutchings, F. Gottschalk and R. Hunter, *Ind. Eng. Chem. Res.*, 1987, **26**, 635–637.
25 M. Bjørgen, U. Olsbye and S. Kolboe, *J. Catal.*, 2003, **215**, 30–44.
26 M. Bjørgen, U. Olsbye, S. Svelle and S. Kolboe, *Catal. Lett.*, 2004, **93**, 37–40.
27 M. Bjørgen, U. Olsbye, D. Petersen and S. Kolboe, *J. Catal.*, 2004, **221**, 1–10.
28 C. D. Chang, *Catal. Rev.*, 1984, **26**, 323–345.
29 F. L. Bleken, T. V. W. Janssens, S. Svelle and U. Olsbye, *Microporous Mesoporous Mater.*, 2012, **164**, 190–198.
30 S. Teketel, W. Skistad, S. Benard, U. Olsbye, K. P. Lillerud, P. Beato and S. Svelle, *ACS Catal.*, 2012, **2**, 26–37.
31 M. Westgård Erichsen, S. Svelle and U. Olsbye, *J. Catal.*, 2013, **298**, 94–101.
32 K. Barbera, F. Bonino, S. Bordiga, T. V. W. Janssens and P. Beato, *J. Catal.*, 2011, **280**, 196–205.
33 S. Teketel, M. Westgard Erichsen, F. Lonstad Bleken, S. Svelle, K. Petter Lillerud and U. Olsbye, in *Catalysis: Volume 26*, The Royal Society of Chemistry, 2014, vol. 26, pp. 179–217.

34 F. Bleken, W. Skistad, K. Barbera, M. Kustova, S. Bordiga, P. Beato, K. P. Lillerud, S. Svelle and U. Olsbye, *Phys. Chem. Chem. Phys.*, 2011, **13**, 2539–2549.
35 R. Castañeda, A. Corma, V. Fornés, J. Martínez-Triguero and S. Valencia, *J. Catal.*, 2006, **238**, 79–87.
36 K. Möller and T. Bein, *Microporous Mesoporous Mater.*, 2011, **143**, 253–262.
37 S. Ernst, J. Weitkamp, J. A. Martens and P. A. Jacobs, *Appl. Catal.*, 1989, **48**, 137–148.
38 S. Brunauer, P. H. Emmett and E. Teller, *J. Am. Chem. Soc.*, 1938, **60**, 309–319.
39 J. Rouquerol, P. Llewellyn and F. Rouquerol, in *Studies in Surface Science and Catalysis*, Elsevier, 2007, vol. 160, pp. 49–56.
40 P. Magnoux, P. Roger, C. Canaff, V. Fouche, N. S. Gnep and M. Guisnet, *Stud. Surf. Sci. Catal.*, 1987, **34**, 317–330.
41 B.-T. Bleken, D. Wragg, B. Arstad, A. Gunnæs, J. Mouzon, S. Helveg, L. Lundegaard, P. Beato, S. Bordiga, U. Olsbye, S. Svelle and K. Lillerud, *Top. Catal.*, 2013, **56**, 558–566.
42 F. J. Keil, *Microporous Mesoporous Mater.*, 1999, **29**, 49–66.
43 M. Sugimoto, H. Katsuno, K. Takatsu and N. Kawata, *Zeolites*, 1987, **7**, 503–507.
44 C. D. Chang, C. T. W. Chu and R. F. Socha, *J. Catal.*, 1984, **86**, 289–296.
45 D. Chen, H. P. Rebo, K. Moljord and A. Holmen, *Ind. Eng. Chem. Res.*, 1997, **36**, 3473–3479.
46 F. L. Bleken, K. Barbera, F. Bonino, U. Olsbye, K. P. Lillerud, S. Bordiga, P. Beato, T. V. W. Janssens and S. Svelle, *J. Catal.*, 2013, **307**, 62–73.
47 S. Teketel, L. F. Lundegaard, W. Skistad, S. M. Chavan, U. Olsbye, K. P. Lillerud, P. Beato and S. Svelle, *J. Catal.*, 2015, **327**, 22–32.
48 P. del Campo, W. A. Slawinski, R. Henry, M. W. Erichsen, S. Svelle, P. Beato, D. Wragg and U. Olsbye, *Surf. Sci.*, 2016, **648**, 141–149.
49 S. Teketel, U. Olsbye, K. P. Lillerud, P. Beato and S. Svelle, *Appl. Catal., A*, 2015, **494**, 68–76.
50 M. Bjørgen, S. Akyalcin, U. Olsbye, S. Benard, S. Kolboe and S. Svelle, *J. Catal.*, 2010, **275**, 170–180.
51 M. Bjørgen, F. Joensen, K.-P. Lillerud, U. Olsbye and S. Svelle, *Catal. Today*, 2009, **142**, 90–97.
52 J. W. Park, S. J. Kim, M. Seo, S. Y. Kim, Y. Sugi and G. Seo, *Appl. Catal., A*, 2008, **349**, 76–85.
53 C. Baerlocher, L. B. McCusker and D. H. Olson, *Atlas of zeolite framework types*, Elsevier, 2007.

